Soft Matter

Layer-by-Layer Assembly of Nanorods on a Microsphere via Electrostatic Interactions

Journal:	*Soft Matter*
Manuscript ID	SM-ART-01-2018-000062.R1
Article Type:	Paper
Date Submitted by the Author:	30-Mar-2018
Complete List of Authors:	Zhang, Liuyang; University of Georgia, College of Engineering Zhu, Lu; University of Georgia, Larson, Steven; University of Georgia, Department of Physics and Astronomy Zhao, Yiping; University of Georgia, Department of Physics and Astronomy Wang, Xianqiao; University of Georgia, College of Engineering

Layer-by-Layer Assembly of Nanorods on a Microsphere via Electrostatic Interactions

Liuyang Zhang[1,2*], Lu Zhu[2*], Steven R. Larson[3], Yiping Zhao[3#] and Xianqiao Wang[2#]

[1] State Key Laboratory for Manufacturing Systems Engineering, Xi'an Jiaotong University, Xi'an, Shaanxi, 710049, China

[2] College of Engineering, University of Georgia, Athens, GA 30602, USA

[3] Department of Physics and Astronomy, University of Georgia, Athens, GA 30602, USA

[*]Co-first authors; [#]Corresponding authors: zhaoy@phys.uga.edu and xqwang@uga.edu

Abstract

Combining coarse-grained molecular dynamics simulations and experiments, a systematic study on both the dynamics and equilibrium behavior of the layer-by-layer (LbL) assembly of charged nanorods (NRs) onto a charged microsphere (MS) *via* electrostatic interactions has been carried out. The adsorption of the first layer of NRs on MS follows a growth-saturation dynamics. The adsorption rate is governed by a diffusion limited process when the NR concentration (C_{NR}) is low; while the rate is independent of C_{NR} when C_{NR} is high. The equilibrium NR coverage on the microsphere is found to follow a Langmuir adsorption model. For multilayer LbL assembly, when C_{NR} is low, the number (N) of NRs adsorbed onto the MS follows a linear relationship with the number (M) of dips; while when C_{NR} is high, in each dip the MS surface is fully covered with NRs, and the N follows a quadratic relationship with M. Most simulation results have been confirmed by experiments using α-Fe_2O_3 NRs and magnetic microspheres modified by poly(diallyldimethylammonium chloride) and poly(styrenesulfonate, sodium salt). These findings provide useful guidelines for designing complex superparticles via charged building nanoblocks based on electrostatic interactions, and therefore open up a novel avenue to exploit the capability of self-assembled charged nanostructures for potential applications such as surface modifications, sensors, drug delivery vehicles, etc.

Keywords: Layer by layer assembly, molecular dynamics, charged nanorods, electrostatic interactions

Introduction

As a versatile fabrication technique, layer-by-layer (LbL) assembly has emerging as a powerful bottom-up method to grow complex nano/micro-structures. This self-assembly method of polycations or polyanions on solid surfaces led to the build-up of multilayer films, which allows different surface modifications to form multifunctional films.[1-3] Thus, the LbL assembly is considered as a method with wide variety of applications in surface modification, sensors, conducting or light-emitting devices, drug delivery vehicles, nanoreactors, and so forth.[4-6] In addition, the LbL assembly is also adopted to form multifunctional superparticles. [7-9] In superparticle fabrication, the oppositely charged small particle components can be absorbed onto a charged core particle alternatively to form a complex and large particle cluster, such as a core-shell structure and a hollow structure. [10] Polymer is one of the most popular charged species adopted in the LbL self-assembly to form superparticles. For example, poly(diallyldimethylammonium chloride) (PDADMAC) and poly(styrenesulfonate, sodium salt) (PSS) polymers were consecutively deposited onto the negatively charged sulphated-stabilized 640 nm Polystyrene (PS) latex particles, then 25 nm SiO_2 nanoparticles were deposited onto the polyelectrolyte-coated PS lattices to form a SiO_2 coating layer on their surfaces. Hollow spheres formed by a layer of SiO_2 nanoparticles were obtained by etching away the PS lattice cores. [11] By using alternating poly (allylamine hydrochloride) (PAH)/PSS/PAH layers, Wang *et al*. coated PS beads in a diameter of 925 nm with the fluorescence CdTe quantum dots (QDs) in diameter of 4 nm. [10] In this work, the CdTe QDs electrostatically interact with PAH through the anionic $-COOH^-$ groups on their surfaces and the cationic $-NH^{3+}$ groups on PAH. The PAH polymer interacts with the PSS polymer because of the negatively charged $-SO^{3-}$ groups on PSS. By tuning the deposition conditions of the polyelectrolytes onto particle surfaces, the LbL technique allows control of coating thickness, coating agents, and product morphologies. [12] These complex superparticles can be designed and functionalized for a specific application. For example, Wang *et al*. fabricated a novel multifunctional Fe_3O_4@C@CdTe microsphere structure with a fluorescent shell and a magnetic core. [13] They demonstrated that these superparticles could be used as a high sensitive and flexible Cu^{2+} ions sensor in aqueous solutions. By coating the oppositely charged Ag nanoparticles onto silica microspheres layer by layer, Yun *et al*. fabricated the SERS-active microsphere-nanoshell structures for trace analysis of crystal violet and SCN^- in aqueous solutions.[14] Serveaux *et al*. successfully fabricated multifunctional

digitally encoded microparticles through LbL coating and spatial selective photobleaching. [15] They demonstrated that the LbL coating layers of CrO_2 nanoparticles on the encoded fluorescence PS beads allows an optimal readout of the codes, perfect orientation accuracy, and an optimal coupling of capture probes to the surfaces due to the ferromagnetic properties of CrO_2 particles. Besides the applications as multifunctional materials, the LbL superparticles have also been introduced to modify living cell surfaces for biological applications.[16-17] For example, Ai *et al*. successfully coated the platelets with silica nanoparticles, fluorescent nanospheres, and bovine immunoglobulin G through LbL assembly.[18] Their work of coating blood cells with organized nanoshells shows the potential of LbL assembly in cardiovascular research and targeted drug delivery. [18] Yang *et al.* also successfully encapsulated individual living yeast cells within silica shells through LbL coating, and this process is also considered as a coating method without harsh reaction conditions to disturb cells. [19] Drachuk *et al*. used functionalized silk polyelectrolytes to form LbL shells onto bacterial surfaces. They demonstrated that the LbL shells with charged polycationic amino acids promoted the formation of cell aggregates; meanwhile the hydrogen-bonded LbL shells promoted the formation of stable colloidal suspensions of individual cell encapsulates.[20]

In order to form these aforementioned self-assembly superparticles, several effects, such as electrostatic forces, hydrogen bonding, hydrophobic interactions, van der Waals forces, the geometry and size of the microparticles/nanoparticles, play important roles in the corresponding LbL assembly process.[21] For these charged building block, electrostatic forces are the dominant and efficient interaction to drive the LbL assembly. Each deposited layer leads to a charge overcompensation that has two important consequences: (i) the repulsion of same charged particles causing self-regulation of their adsorption and restriction to a single layer and; (ii) the formation of a new layer by the adsorption of oppositely charged building blocks on the top of the previous layer.[21] Though many reports have shown that the LbL electrostatic strategy is a promising method to engineer functional superparticles, [10-12, 22] the fundamental understanding of the formation mechanism, the product structure, and the effect of the property of each building block is still lagging behind,[23] especially very few theoretical and simulation studies at the microscopic level have been reported. Molecular dynamics simulations offer an alternative way to investigate the underlying mechanism of the self-assembly process at the microscale level. [24-27] For example, the simulation work of the LbL assembly of charged nanoparticles on porous

substrates by Carrillo *et al*. revealed that the layer assembly proceeded through surface overcharging during each deposition step, and both the layer thickness and the surface coverage of the film increased linearly with the number of deposition steps.[5] However, the effects of the charged particle concentration, size and shape of the core particle or particle used to assemble still remain unknown for superparticle formation. In this paper, we will investigate the LbL assembly process of complex superparticle formation with a charged microsphere (MS) as a substrate and charged nanorods (NRs) as building blocks using both coarse-grained molecular dynamics simulations and experiments. The charged nanorod dynamics under a single layer and the multilayer formation under equilibrium deposition are studied. Effects of nanoparticle concentration, charge density, and shape of NRs on their final assembled structures will be elaborated. The results from both molecular dynamic simulations and experiments agree fairly well, demonstrating the effectiveness of our molecular dynamic models, which can be used for further investigations such as the effect of charge density, nanorod shape, size as well as the core particle size and shape. Our study shows that the coarse-grained molecular dynamic simulation is an excellent tool to understand the LbL process.

Simulations and Experiments

Simulation Details

We used a coarse-grained molecular dynamics model called stochastic rotation dynamics (SRD) to perform all simulations in this work.[28-29] SRD is a member of techniques referred to as multi-bead collision dynamics that attempt to efficiently resolve important mesoscale phenomena, such as fluctuating hydrodynamics, momentum conservation, and self-assembly at the cost of microscopic information.[29-30] The NRs, MS, and solvent particles are modeled by and composed of SRD beads (Figure 1). SRD bead is a sizeless particle with a unit mass and charge. A reduced unit system is adopted, and the mass, length, time, charge, and energy units are all normalized, with the unit of mass to be that of SRD bead m_0, the unit of length taken to be reduced length σ, the unit of time to be reduced time τ, the unit of charge to be the reduced charge e, and the unit of energy to be k_BT (k_B is Boltzmann constant, T is temperature). Unless otherwise stated, a single ellipsoidal NR (major axis length $d_{NR}^{major} = 7.4\sigma$, minor axis length $d_{NR}^{minor} = 1.44\sigma$) is composed of 50 SRD beads with charge $q_{nr} = +10e$ on each SRD bead while the spherical MS (radius $r_{MS} = 19.3\sigma$) contains 30,186 SRD beads with $q_m = -1e$ on each SRD bead. A solvent

particle is made of one SRD bead with no charge.

The simulation box with a dimension of $44\,\sigma\,(x) \times 44\,\sigma\,(y) \times 44\,\sigma\,(z)$ has periodic boundary conditions in all three directions. The MS is placed at the center of simulation box and NRs are uniformly and randomly distributed in the simulation box initially. Assuming the total number of NRs in the solvent keeps constant. The NRs, MS, and solvent particles in the system interact through the 12-6 Lennard Jones (LJ) potentials

$$\boldsymbol{U_{LJ}(r_{ij}) = 4\epsilon\left[\left(\frac{b}{r_{ij}}\right)^{12} - \left(\frac{b}{r_{ij}}\right)^{6}\right],\quad r_{ij} < r_c = 3b}\,, \tag{1}$$

where r_{ij} is the distance between i^{th} and j^{th} beads, and $\epsilon = 1\,k_BT$ and $b = 1\,\sigma$ are the depth of the potential well and the finite distance at which the inter-bead potential is zero, respectively. Electrostatic interaction between any two charged SRD beads (in NR or in MS or between NRs and MS) with charge value q_i and q_j, and separated by a distance r_{ij} is given by the Coulomb potential

$$\boldsymbol{U_{Coul}(r_{ij}) = \frac{Gq_iq_j}{\varepsilon_0 r_{ij}}}\,, \tag{2}$$

where G is an energy-conversion constant and $\boldsymbol{\varepsilon_0}$ is the dielectric constant. The particle-particle particle-mesh (PPPM) method is used to calculate the electrostatic interactions. We use a velocity-Verlet algorithm to perform time integration, and the time step for integration is $\Delta t = 0.01\tau$. NRs and MS are treated as independent rigid bodies, and the total force and torque on each rigid body are computed as the sum of forces and torques on its constituent SRD beads. The coordinates, velocities, and orientations of the SRD beads in each NR and MS are then updated so that they can move and rotate as a single entity. All LbL self-assembly simulations are performed using the LAMMPS package.[31]

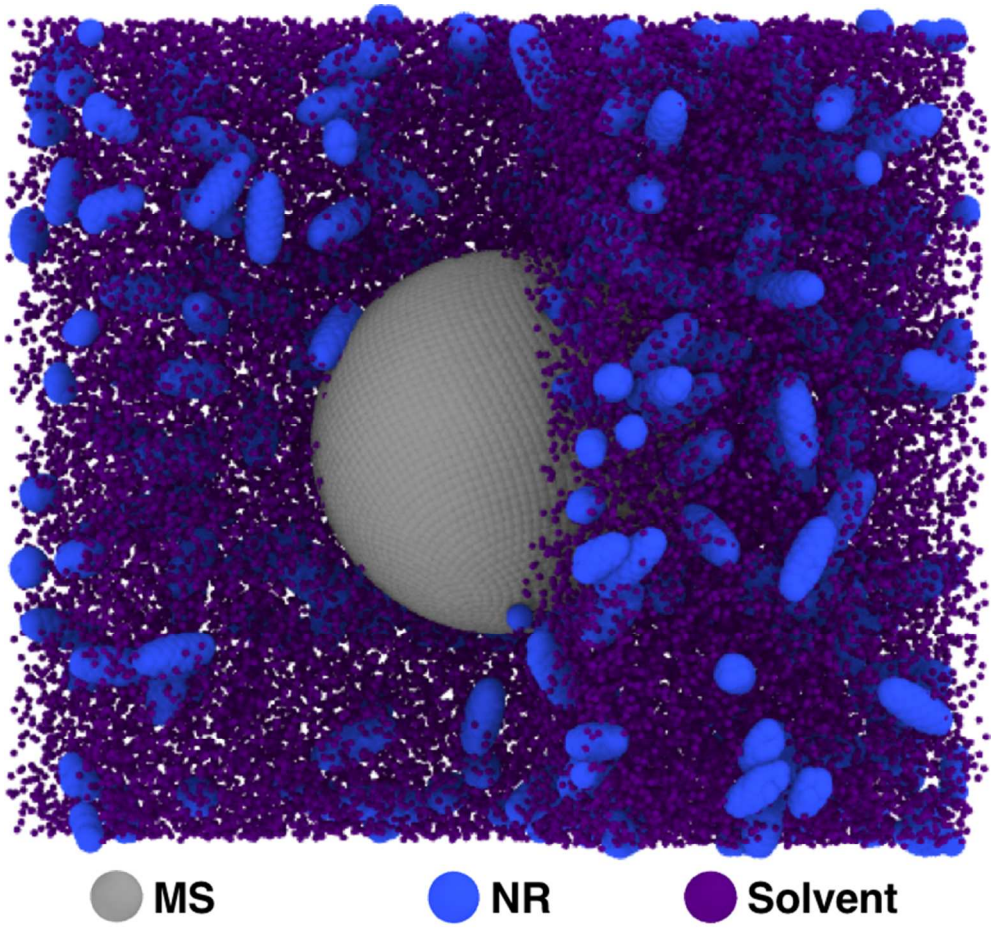

Figure 1. Schematic representation of the simulation model. The SRD beads in the MS, NRs and solvent particles are shown in grey, blue, and purple, respectively. For clarity, the solvent beads are not shown in the following figures.

Experiments

Nanorods Fabrication

Fe_2O_3 NRs were produced through a hydrothermal synthesis method. Briefly, 75 mL 0.02 M $FeCl_3 \cdot 6H_2O$ (Acros Organics) and 0.45 mM NaH_2PO_4 (Sigma) aqueous solutions were completely mixed and then transferred into a 100-mL autoclave. After being maintained at 160 ℃ in an oven for 12 h and cooled down to room temperature, the resulting Fe_2O_3 NRs were collected and washed by centrifugation. The morphology of the Fe_2O_3 NRs was investigated by a field-emission scanning electron microscope (FESEM) equipped with an energy dispersive X-ray spectroscope (FEI Inspect F). As shown in the SEM image in Figure 2(A), the products are uniformly ellipsoidal NRs with a mean length of 370 ± 30 nm and a mean width of 72 ± 6 nm.

The crystal structure of the Fe_2O_3 NRs was characterized by an X-ray diffractometer (XRD; PANalytical X'Pert PRO MRD) with a Cu Kα source (λ = 1.5405980 Å) at 45 kV and 40 mA. The XRD pattern shown in Figure 2(B) demonstrates the hematite crystal structure.

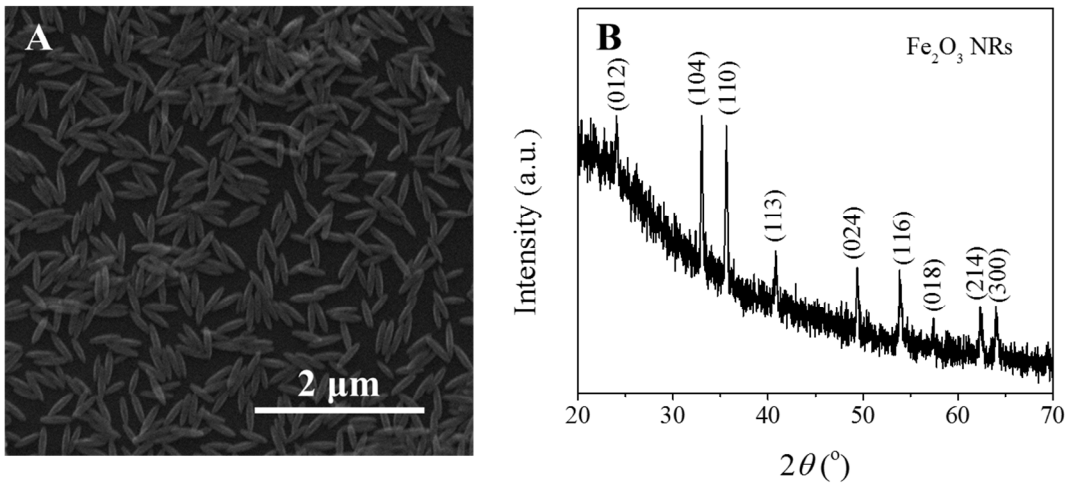

Figure 2. (A): SEM image of as synthesized α-Fe_2O_3 NRs. (B): XRD pattern of as synthesized α-Fe_2O_3 NRs.

Surface Modification

Poly(styrene sulfonate) (PSS) and poly(diallyldimethylammonium chloride) (PDADMAC) were used to introduce the negative and positive charges onto the NRs. PSS was used as the first layer. A 1 ml Fe_2O_3 NR suspension with a concentration of 1 mg/ml was added into 10 ml of 1 mg/ml PSS polyelectrolyte solution containing 0.5 M NaCl. After 30 min, the PSS-Fe_2O_3 NRs were washed with deionized (DI) water twice by centrifugation. The resulting PSS-Fe_2O_3 NRs were then mixed with 10 ml 1mg/ml PDADMAC polyelectrolyte solution containing 0.5 M NaCl for 30 min to obtain the positively charged PDADMAC-PSS-Fe_2O_3 NRs. The coverage of the polyelectrolyte on the particle surfaces affects the particle mobility. [32-33] The surface charge density of the coated MS and NR are also dependent on the coatings of polyelectrolytes, which would directly affected the absorption of the NRs onto MS during the LbL process. The superparamagnetic microspheres (COMPEL™, 3μm) were first washed twice with DI water to remove the surfactants on the surface. Then they were coated first by PDADMAC and second by PSS to ensure the negative surface charge of the microspheres. Zeta-potential measurements of polymer-coated NRs and microspheres were carried out on a Malvern Zetasizer Nano ZS system

at 25 °C. The values are summarized in Table 1. PSS-Fe_2O_3 NRs and the microspheres are dominated by the negative charge, and the PDADMAC-PSS-Fe_2O_3 NRs are shown to be positively charged.

Table 1. Zeta potential of NRs and MS coated with different polymers.

Sample	Zeta potential (mV)
PSS-Fe_2O_3	-48.2
PDADMAC-PSS-Fe_2O_3	62.8
Coated MS	-47.6

LbL NR Deposition on MS

A. Single layer deposition

The one layer NR deposition was performed with the positively charged PDADMAC-PSS-Fe_2O_3 NRs and the negatively charged microspheres. 100 μl microspheres (solid, 0.01 wt.%) was added into a 1 ml NR suspension with different NR concentration c_{NR} (c_{NR} = 0.1 mg/ml, 0.2 mg/ml, 0.3 mg/ml, 0.5 mg/ml, 0.6 mg/ml, 0.8 mg/ml, 1.0 mg/ml, 1.2 mg/ml, and 1.5 mg/ml). The mixtures were shaken for 2 min. Then the superparamagnetic microspheres were separated by a magnet for 5 min and washed once by DI water with low speed vortexing. Time dependent 1st layer deposition was conducted with 0.2 mg/ml and 1.0 mg/ml NRs suspensions at different dipping time (2 min, 10 min, 30 min, 60 min, and 120 min). The numbers of NRs adsorbed on the microsphere surfaces were manually counted based on the SEM images.

B. Multilayer deposition

Multilayer NP deposition was performed with the positively charged PDADMAC-PSS-Fe_2O_3 NRs, PSS-Fe_2O_3 NRs, and the negatively charged microspheres. 20 μl microspheres was firstly added into 200 μl PDADMAC-PSS-Fe_2O_3 NRs suspension with a concentration of 1 mg/ml and shaken for 2 min. Then the microspheres were separated by a magnet, washed twice, and re-suspended into 20 μl DI water. Then, they were added into 200 μl PSS-Fe_2O_3 NRs suspension with a concentration of 1 mg/ml to perform the coating process. These steps were repeated till the 10th dipping cycle.

Results and Discussions

Single Layer NR Deposition

In our simulations, we first study the NR-MS time evolution process as a function of c_{NR} from c_{NR} = 0.1 mg/ml to c_{NR} = 1.5 mg/ml. Figure 3(A) shows the equilibrium configurations of NRs on the MS for different c_{NR}. When c_{NR} is relatively low (*i.e.* $c_{NR} = 0.1$, 0.2, 0.3 mg/ml), NRs adhere sparsely on the MS surface. When c_{NR} is relatively high (*i.e.* $c_{NR} = 1$, 1.2, 1.5 mg/ml), the separation distance between neighboring NRs on the MS surface significantly reduces, and the NR contact or overlap become significant. It is also observed that the NRs self-align into line patterns (*i.e.* $c_{NR} = 0.8$ mg/ml) or hexagonal patterns (*i.e.* $c_{NR} = 1$ mg/ml) on the MS surface (as indicated by yellow solid lines in Figure 3(A)). These patterned structures may minimize the electrostatic interaction energy between the positive charged NRs and the MS. Due to the electrostatic repulsive interaction, two adjacent NRs on the MS surface can adjust their relative positions to make room for accommodating more free NRs from the solvent (more details please see the Supplement Materials). They can also rotate with respect to neighboring NRs to achieve a uniform NR distribution on the MS surface. The structural pattern of NRs on the MS surface can be well characterized by the averaged shortest separation distance between any two NRs adsorbed on MS, d,

$$\boldsymbol{d} = \frac{\mathbf{1}}{\boldsymbol{N}} \sum_{\boldsymbol{i=1, j=1, i \neq j}}^{\boldsymbol{n}} \mathbf{min} \quad ||\vec{\boldsymbol{r}}_{\boldsymbol{i}} - \vec{\boldsymbol{r}}_{\boldsymbol{j}}|| \,, \tag{3}$$

where N is the number of NRs on the MS surface, r_i is the positon vector of a NR i from the center of the MS. The averaged shortest distance between NRs shown in Figure 3(B) monotonically decrease with the increase of c_{NR}, which is in good agreement with the high packing density of NRs on the MS surface as shown in Figure 3(A).

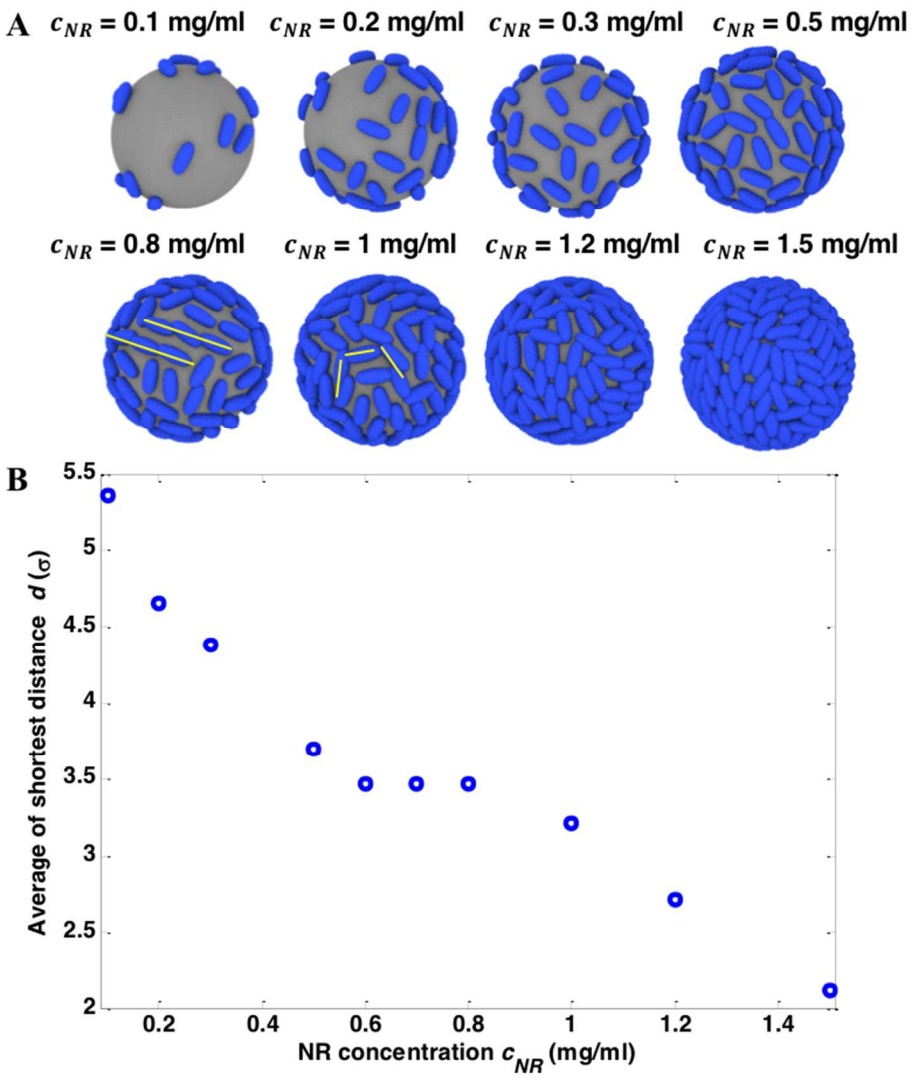

Figure 3. (A) Snapshots of the equilibrium state of the NRs-MS system under various NR concentrations. The yellow solid lines highlight self-organized NRs on the MS surface. (B) the plot of the averaged shortest distance $\boldsymbol{d}$ among NRs with respect to NR concentration $\boldsymbol{c_{NR}}$

Figure 4(A) presents the time evolution of the number of ellipsoidal NRs N adsorbed on the MS surface under varying c_{NR}. Each evolution process roughly consists of two stages. The first stage is the adsorption stage, in which the number of NRs adsorbed on the MS increases rapidly. The adsorption stage is mainly governed by the interplay of electrostatic and van der Waals interactions between the negatively charged MS and positively charged NRs. The repulsive

electrostatic interactions between positively-charged NRs in the solvent also contributes to drive free NRs approaching the negatively-charged MS. In this adsorption stage, the MS is gradually neutralized by the oppositely charged NRs via direct attachment. The second stage is the equilibrium stage, when the number of NRs on the MS surface gradually reaches a steady-state value. For example, at c_{NR} = 1.5 mg/ml, the MS can adsorb up to 180 NRs on its surface while at c_{NR} = 0.1 mg/ml, it can adsorb up to 15 NRs, which indicates that a saturation state of NR adsorption on the surface of MS heavily depends on the NR concentration. This saturation stage of the NRs-MS system is mainly governed by the competition of the electrostatic attraction between free NRs in the solvent and the gradually neutralized MS, and the electrostatic repulsion among free NRs in the solvent. The interaction between NRs and the MS is also analyzed during the entire deposition process. From the time evolution of interfacial binding energy U between NRs and the MS in Figure 4(B), the initial sharp decline indicates a quick adsorption of NRs on the MS surface. Then, the interfacial binding energy gradually decreases as more NRs adsorb onto the MS surface. The energy plateau corresponds to the saturation stage of NR adsorption. The negative sign of the interaction energy indicates that the state where NRs are adsorbed on the MS surface is energetically favorable. The energy profile can further support the synchronous time evolution of the number of NRs on the MS surface as shown in Figure 4(A).

Theoretically, the number of NRs N adsorbed onto a MS can be fit by a kinematic function,

$$\boldsymbol{N = N_{\infty} * \left(1 - e^{-k_0 t}\right)}, \tag{4}$$

where k_0 is the adsorption constant, and N_∞ represents the maximum number of NRs that can be adsorbed on the MS. The fitting results are shown by the dashed curves in Figure 4(A). In general, Eq. (4) fits the simulation results very well. Figure 5 shows the relationship between k_0 and c_{NR}. For different c_{NR}, the overall adsorption process could either belong to a diffusion limited process or a reaction limited process. For a diffusion limited process, the adsorption rate k_0 should linearly increase with c_{NR} while for a reaction limited process, k_0 should gradually approach to a constant. As demonstrated by Figure 5, when $c_{NR} \leq 0.8$ mg/ml, k_0 increases linearly with c_{NR}, indicating a diffusion limited process; while for $c_{NR} > 0.8$ mg/ml, the k_0 is almost independent of c_{NR}, a reflection of the reaction limited process.

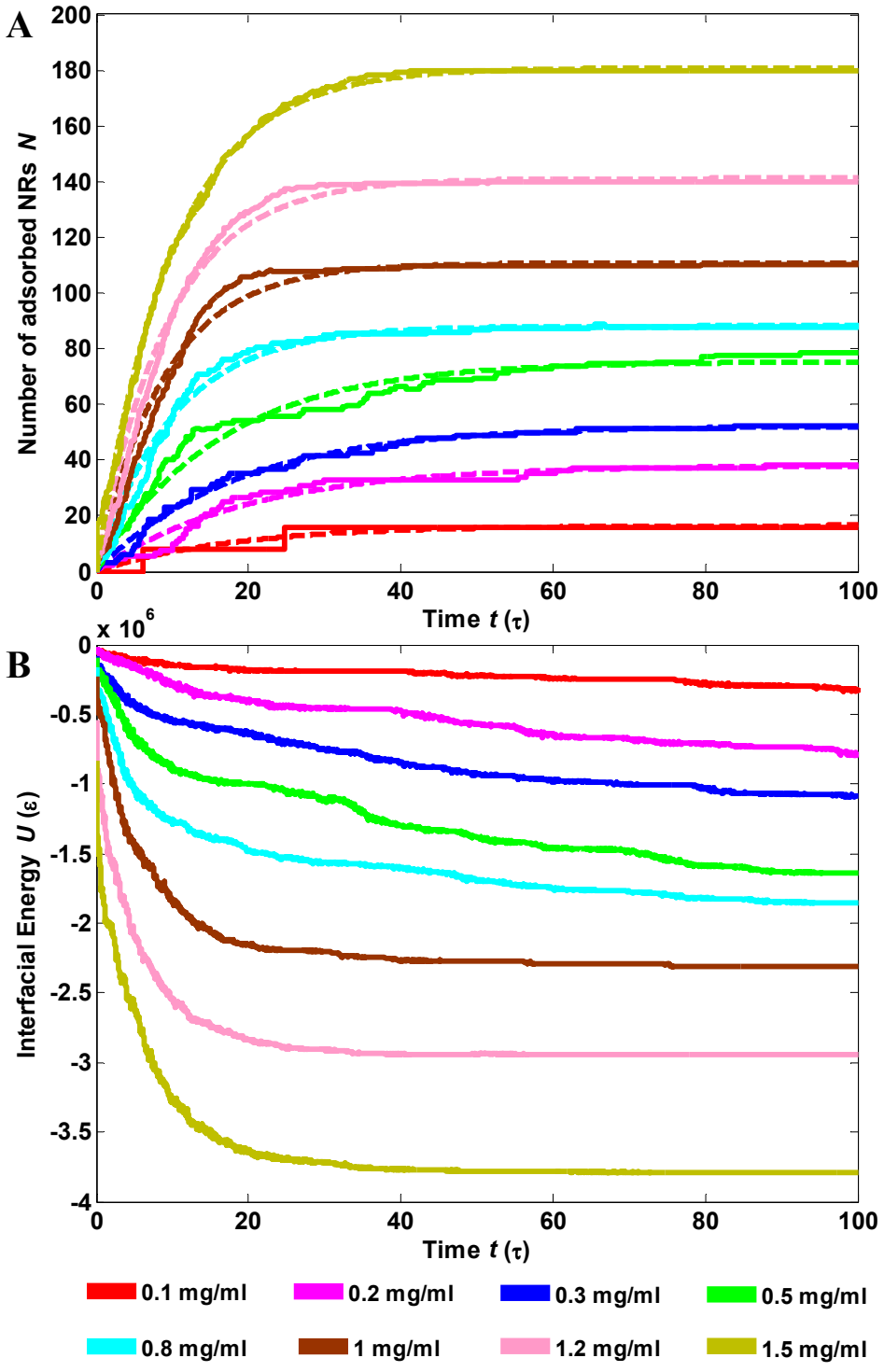

Figure 4. (A) Time evolution of the number of NRs adsorbed onto the MS surface. The solid line represents the simulation result and the dash line represents the fitting result. (B) Time evolution of the interfacial energy ***U*** between NRs and MS.

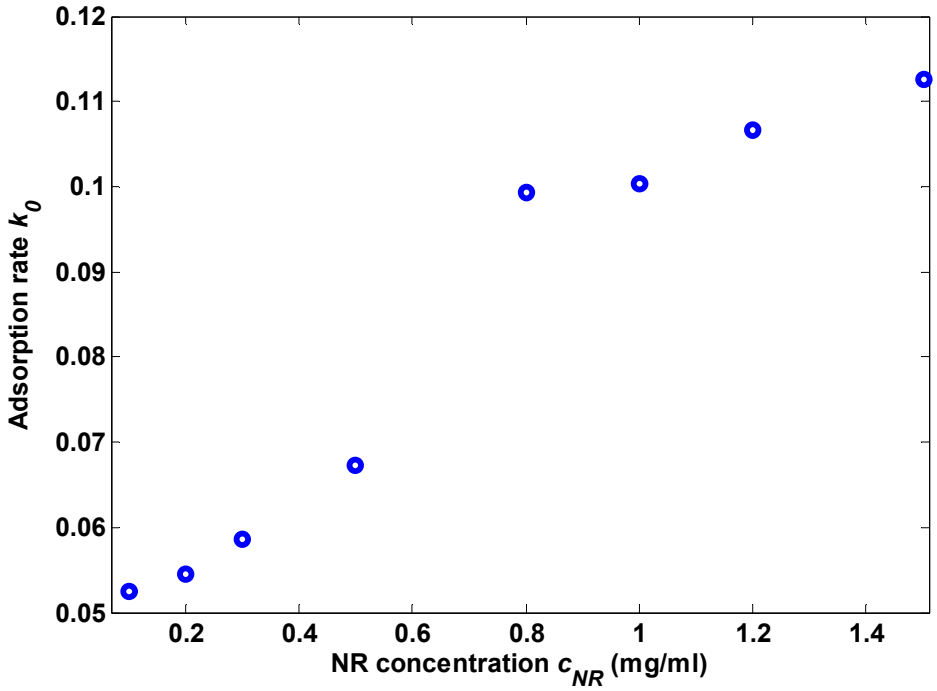

Figure 5. The plot of adsorption constant $\boldsymbol{k_0}$ with respect to NR concentration $\boldsymbol{c_{NR}}$.

To confirm the simulation results, a time-dependent single layer NR deposition experiment was performed, and the c_{NR} = 0.2 mg/ml and c_{NR} = 1.0 mg/ml suspensions were analysed. The representative SEM images of the MS in Figure 6(A) for t = 2 min to t = 120 min show that multiple NRs are adsorbed on the MS. While most NRs lie flat on the MS surface, as predicted in Figure 3(A), few are actually protruded out from the surface. But the self-alignment of the NRs predicted by simulations is not observed, which could be due to the relative low coverage of NRs on the MS surface. Figure 6(B) plots the number of NRs adsorbed on MS (N) as a function of time t. Despite of NR concentration, N barely changes for the deposition time, which means for these two NR concentrations and within the 2-minute period, the system can reach the equilibrium stage as discussed in Figure 4, and the time for the diffusion stage is very short, *i.e.*, $k_0 < 0.5$ min^{-1}. Such a fast adsorption process could help the MS surface modification in certain specific applications.

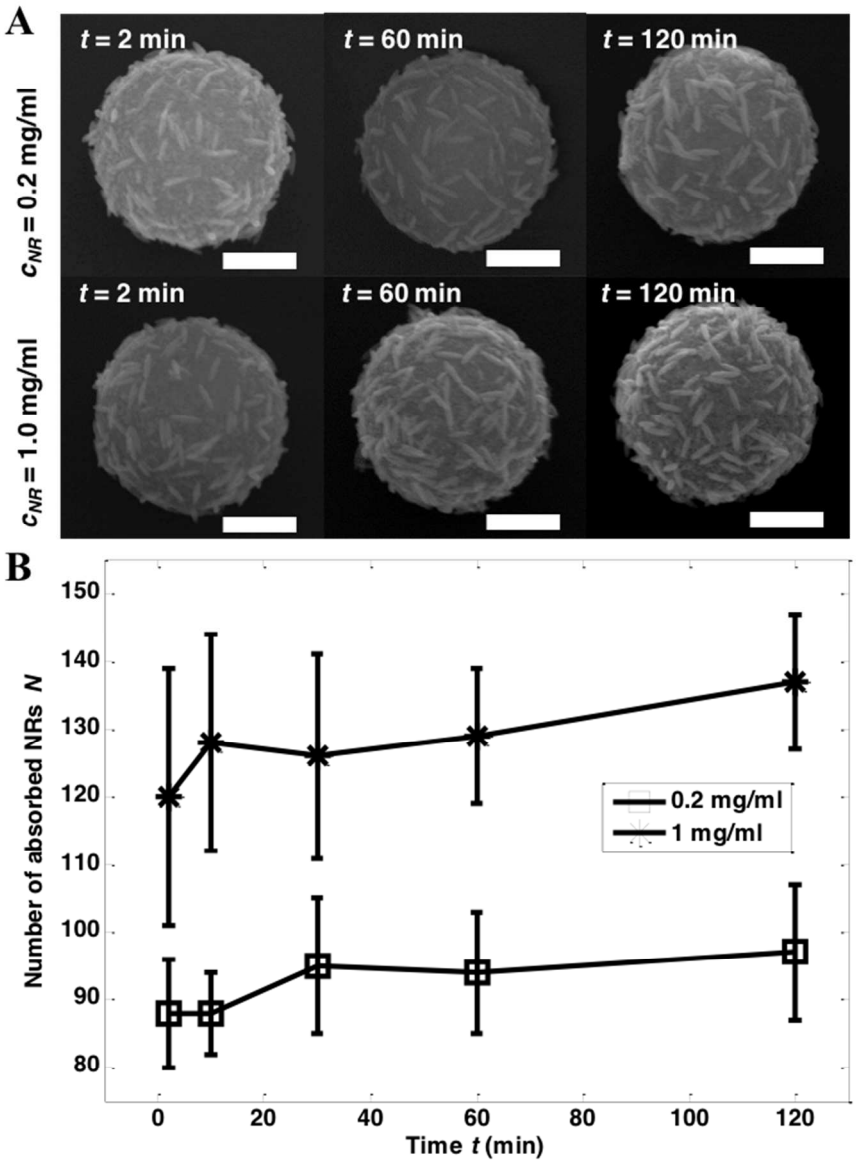

Figure 6. Time-dependent single layer NR deposition on a MS surface: (A) Respective SEM images of the coated microspheres under different coating time. The scale bar for all images is 1 μm. (B) the plot of the number ***N*** of adsorbed NRs on MS versus deposition time.

Theoretically, the NR adsorption on the MS surface can be further explained by a classical Langmuir adsorption model. The MS can be assumed to be an ideal flat solid surface composed of distinct sites capable of binding NRs. Once an NR with finite size attaches onto the MS surface, we consider that an adsorption site on the MS is occupied. The surface coverage θ, defined as the ratio of the projection area of adsorbed NRs on the MS surface to the total surface

area of the MS, follows the Langmuir adsorption model,

$$\boldsymbol{\theta} = \frac{\boldsymbol{bc_{NR}}}{\boldsymbol{1+bc_{NR}}} , \quad (5)$$

where b is a temperature-dependent equilibrium constant and related to the Gibbs free energy (and hence to the enthalpy change) for the deposition process. Figure 7 shows the θ versus c_{NR} plot obtained from the simulations. By fitting the data using Eq. (5) where $b = 1.18 \pm 0.02\ ml/mg$, the fitting curve follows the simulation data relatively well. It can be predicted that after the critical saturation concentration (c_{NR} = 1.5 mg/ml), NR adsorption does not occur, *i.e.*, there is no vacancy left on the surface of MS for a NR to be adsorbed.

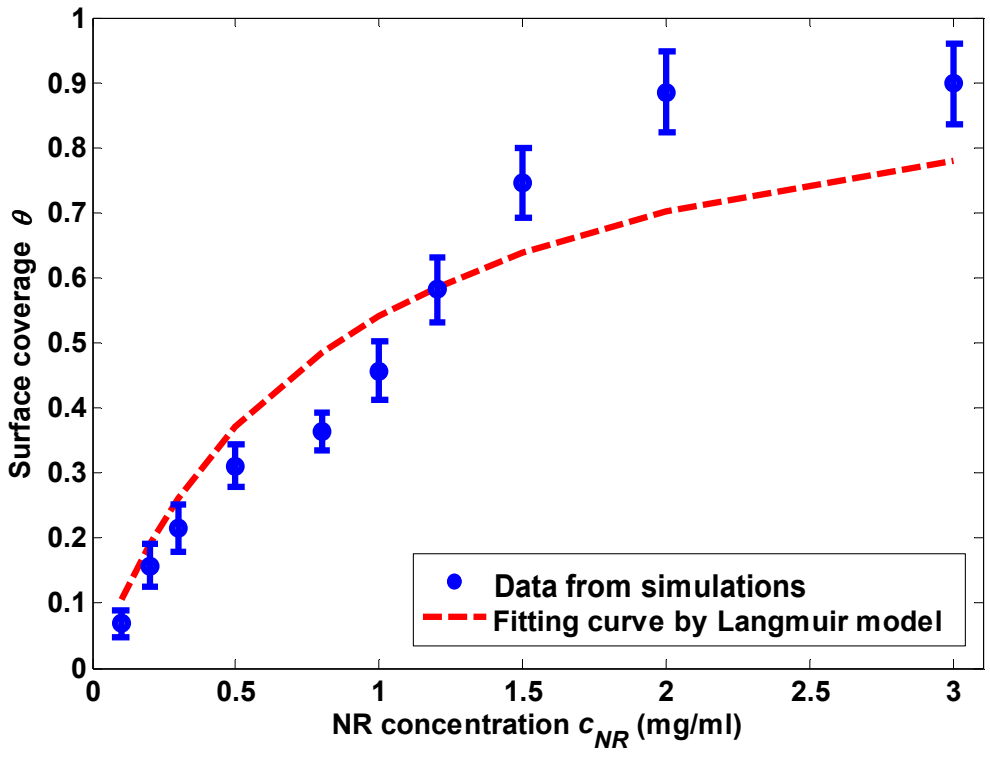

Figure 7. The plot of the surface coverage $\boldsymbol{\theta}$ versus NR concentration $\boldsymbol{c_{NR}}$: simulation data and fitting curve based on the Langmuir adsorption model.

Experimentally, a NR concentration-dependent single layer adsorption validation was performed. The SEM images of the representative MS coated with NRs are shown in Figure 8(A). The images indicate that with the increase of c_{NR}, the number of adsorbed NRs on the MS gradually increases. Figure 8(B) plots N versus c_{NR}. The large error bars on the data points indicate large

uncertainty in NP counting (an average of more than 10 MS particles). By assuming that $\theta \propto N$, this N- c_{NR} data can be fitted by a modified Eq. (5), $N = \frac{ac_{NR}}{1+bc_{NR}}$. One can obtain that $a = 2100 \pm 100\, ml/mg$ and $b = 18.1 \pm 0.2\, ml/mg$. As shown by the dashed curve in Figure 8 (B), the fitting curve follows the experimental data relatively well. And when the c_{NR} = 1 mg/ml, N reaches a saturation value. Similar time-dependent LbL assembly trends are observed in both experiments and simulations.[5, 34]

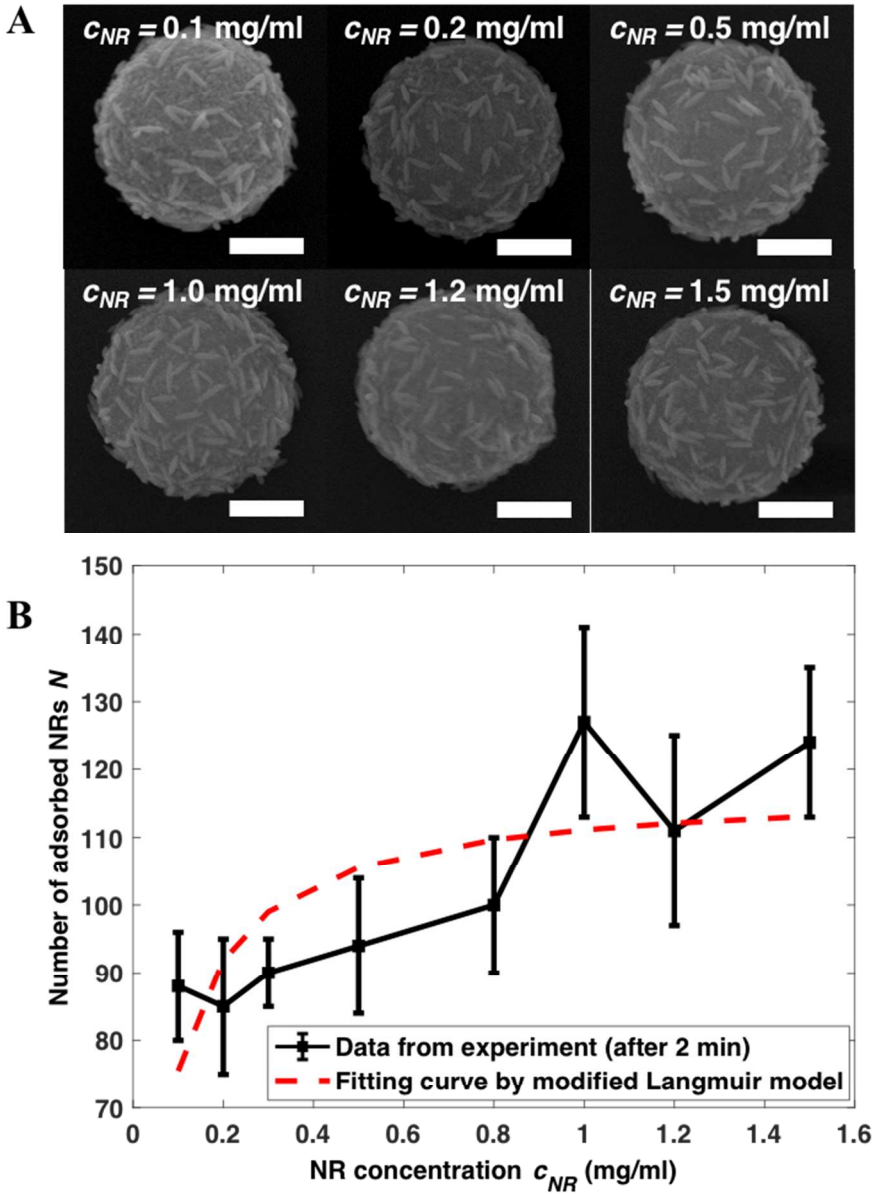

Figure 8. Concentration dependent single layer NRs deposition on MS: (A) Representative SEM images of NRs coated MS for different c_{NR} under equilibrium stages. The scale bar for all

images is 1 μm. (B) The plot of the number $\boldsymbol{N}$ of adsorbed NRs on MS versus $\boldsymbol{c_{NR}}$ under equilibrium stages.

Multilayer NR Deposition

Based on the understanding of the behavior of the single layer adsorption, we follow the abovementioned procedure to implement a sequential multilayer deposition of charged NRs. Figure 9 shows snapshots of the equilibrium multilayer structure after M = 1 to 5 dips for c_{NR} = 0.3 mg/ml, 1 mg/ml, and 2 mg/ml, respectively. The duration of each dip is sufficiently long ($\sim 150\ \tau_0$) such that the system reaches the equilibrium state, as discussed in Figure 3. After each dip, the layer thickness of the equilibrium structure increases. In order to maintain approximately the same accessible volume to the MS surface we need to adjust the simulation box size for each dip to. Also, the unadsorbed NRs after the completion of each dip are separated from the adsorbed ones using a cluster algorithm with a cut-off radius 2.0 σ. The cluster analysis is performed by calculating the positions of all NRs on the MS surface. Such a process mimics the rinsing process and ensures an accurate identification of the adsorbed NRs. As shown in Figure 9, the multilayer LbL process strongly depends on c_{NR}. When c_{NR} (= 0.3 mg/ml) is small, after the first dip, the surface coverage θ is small, and there are sparse but large voids left on the MS surface. During the second dip, when the simulation box is refilled with oppositely charged NRs (-) with the same c_{NR}, and the negatively charged NRs are adsorbed right on top of the first layer of NRs, and are aligned with the NRs of the first layer. Such an assembly creates a sufficient energy barrier preventing NRs from further being adsorbed onto the first layer. Addition negatively charged NRs do not adhere to the MS surface due to the electrostatic repulsion between negative charges. For the third dip, positive NRs (+) starts to enter these voids left on the MS surface during the first two dips and NRs coagulate onto the second layer as well as the MS surface. As the dip process proceeds further, the number of NRs accumulating onto the MS surface increases, and the coated NRs layers becomes porous and rough. However, when c_{NR} (= 2 mg/ml) is large, even after the first dip, the first layer of NRs almost fully covers the entire MS surface, *i.e.*, $\theta \approx 1$. This newly formed layer provides a newly charged surface for the negatively charged NRs in the next dip. Under this circumstance, the new NRs form a patterned layer which does not strictly adhere to the orientation of NRs of the first layer as we observe under a small NR concentration. Further dips almost create a similar high coverage, and the MS is fully

wrapped by NRs one layer at a time. Figure 10(A) quantitatively shows the number of NRs on the MS surface along with the number of dips M. Based on the Langmuir adsorption model, for a fixed c_{NR}, the equilibrium θ is fixed. Thus, according to our observation, when c_{NR} is small, after each dip, θ is small. Assuming that after each dip, there are still open spaces on MS left for NRs to be adsorbed in the next dip, then $N \propto M$, *i.e.*, N would increase linearly with M as evidenced in Figure 10(A) for c_{NR}= 0.3 mg/ml. However, for a large enough c_{NR}, like c_{NR} = 1mg/ml or c_{NR}= 2 mg/ml, after each dip, $\theta \approx 1$. If we assume that all the major axes of NRs are tangent to the MS surface, then $N \propto (r_{MS} + Md')^2$, where d' is the width of NR, i.e., N is a quadratic function of M. As shown in Figure 10(A) for c_{NR} = 1mg/ml or c_{NR}= 2 mg/ml, the quadratic function fits (dash curves) the simulation data well.

In Figure 10(B), the average thickness of the NR layer $\langle h \rangle$, calculated as the average value of the height distribution of NRs on the MS surface, is plotted as a function of M. For different c_{NR}, a linear relationship is revealed. However, the assembly become slightly thicker (7.3σ) when c_{NR} = 2 mg/ml than that (6.83σ) when c_{NR} = 0.3 mg/ml or c_{NR} = 1 mg/ml after 5 dips. The thickness has negligible difference for varying concentrations. Our LbL assembly simulation demonstrates similar features to those observed for assembly of charged nanoparticles on a porous substrate.[5]

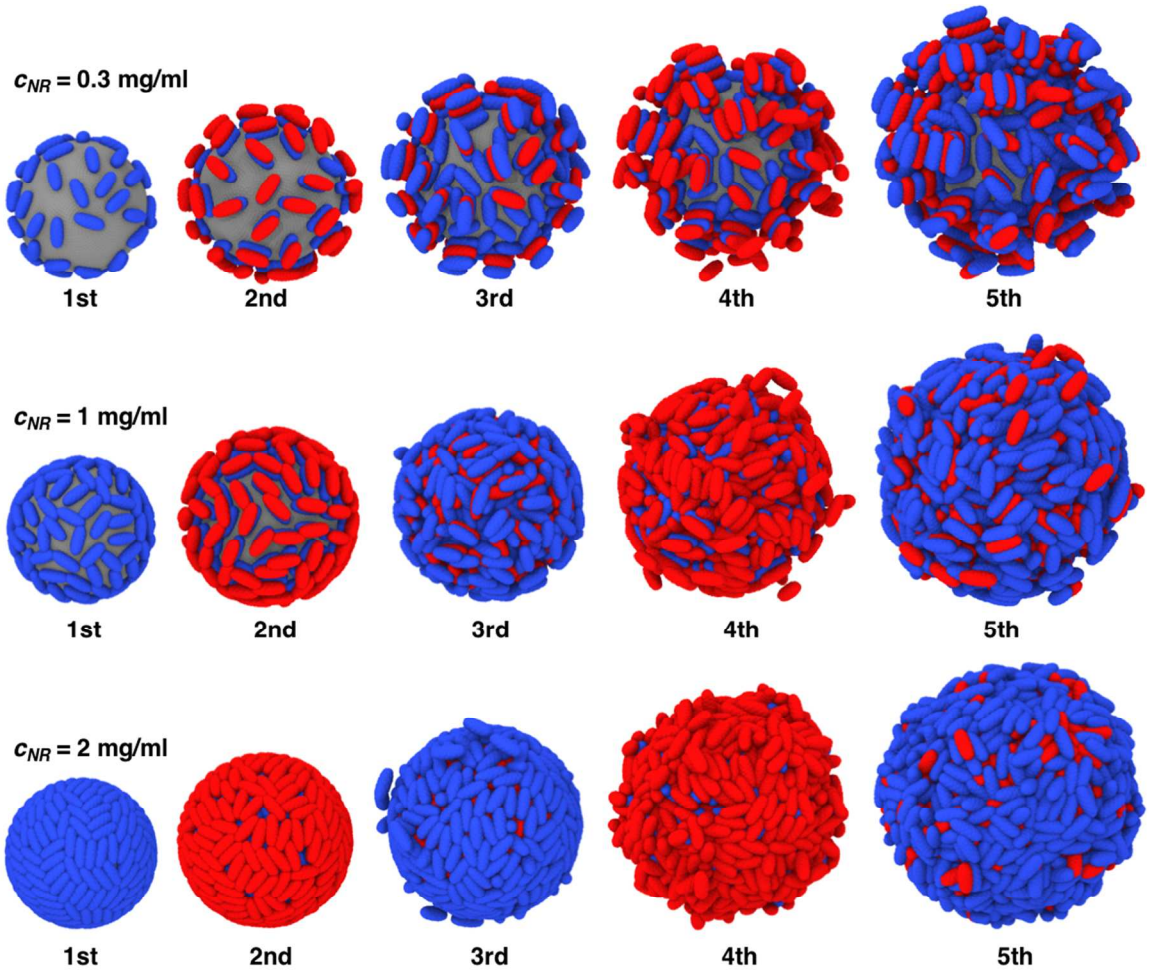

Figure 9. Snapshots of multilayer NRs deposited on MS for c_{NR} = 0.3 mg/ml, 1 mg/ml, and 2 mg/ml, respectively. The blue NRs are positively charged while the red NRs are negatively charged.

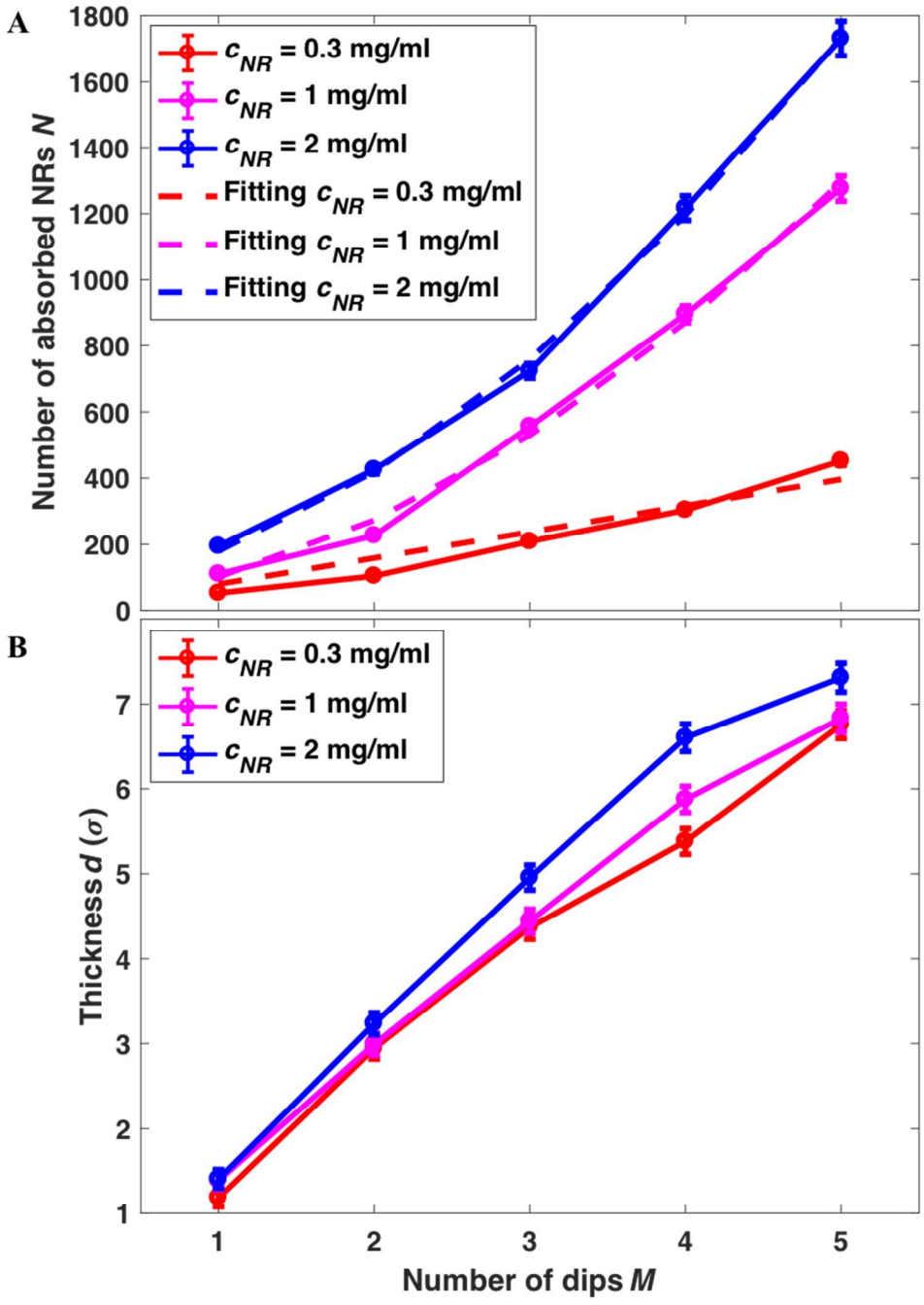

Figure 10. Multilayer NR deposition on the MS surface with respect to the number of dips: (A) the number $\boldsymbol{N}$ of NRs on MS versus the number of dips $\boldsymbol{M}$. The solid line represents the simulation result and the dash line represents the fitting result. For $\boldsymbol{c_{NR}}$ = 0.3mg/ml, using linear fitting function ($\boldsymbol{N = a_1 M}$) where $\boldsymbol{a_1 = 79.33}$; For $\boldsymbol{c_{NR}}$ = 1 mg/ml, using quadratic fitting function ($\boldsymbol{N = a_2 M^2 + b_2 M}$,) where $\boldsymbol{a_2 = 40.41}$ and $\boldsymbol{b_2 = 56.37}$; For $\boldsymbol{c_{NR}}$ = 2 mg/ml, using

quadratic fitting function ($\boldsymbol{N = a_3 M^2 + b_3 M}$,) where $\boldsymbol{a_3 = 45.70}$ and $\boldsymbol{b_3 = 117.41}$. (B) the thickness $\langle \boldsymbol{h} \rangle$ of NRs-MS hybrid structure versus the number of dips $\boldsymbol{M}$.

The corresponding experimental SEM images are shown in Figure 11(A) with c_{NR} = 1 mg/ml. With the increase of M, the number of adsorbed NRs on the MS surface increases, which is qualitatively consistent with the simulation results. However, under the experimental condition, the surface coverage θ is much smaller than unity. In fact, the SEM images are similar to the situation of c_{NR} = 0.3 mg/ml in Figure 9. Figure 11(B) plots the number N of NRs on MS versus the number of dips M. As expected, N increases almost linearly with M, with a linear fitting $N = aM + b$, where $a = 10.96$ and $b = 110.60$. Clearly, the experimental results do not match with those reported in simulation for c_{NR} = 1 mg/ml (Figure 10 (A)). The discrepancy can be attributed to the following reasons. First, the charged polymer layer coated onto both NRs and MS surfaces used in our experiments may be heterogeneous, causing a possible non-uniform NR deposition on the MS surface. This potential non-uniformity may lead to a noticeable discrepancy in the number of NR adsorbed on MS surface since only one side of the MS is shown under SEM images and used for the NR counting. Second, during the experimental rinsing process between dips, a certain amount of loosely adsorbed NRs might be washed off from the surface of the microsphere while in our simulations we do not consider this scenario. However, the experimental results do agree well with low coverage MS situation.

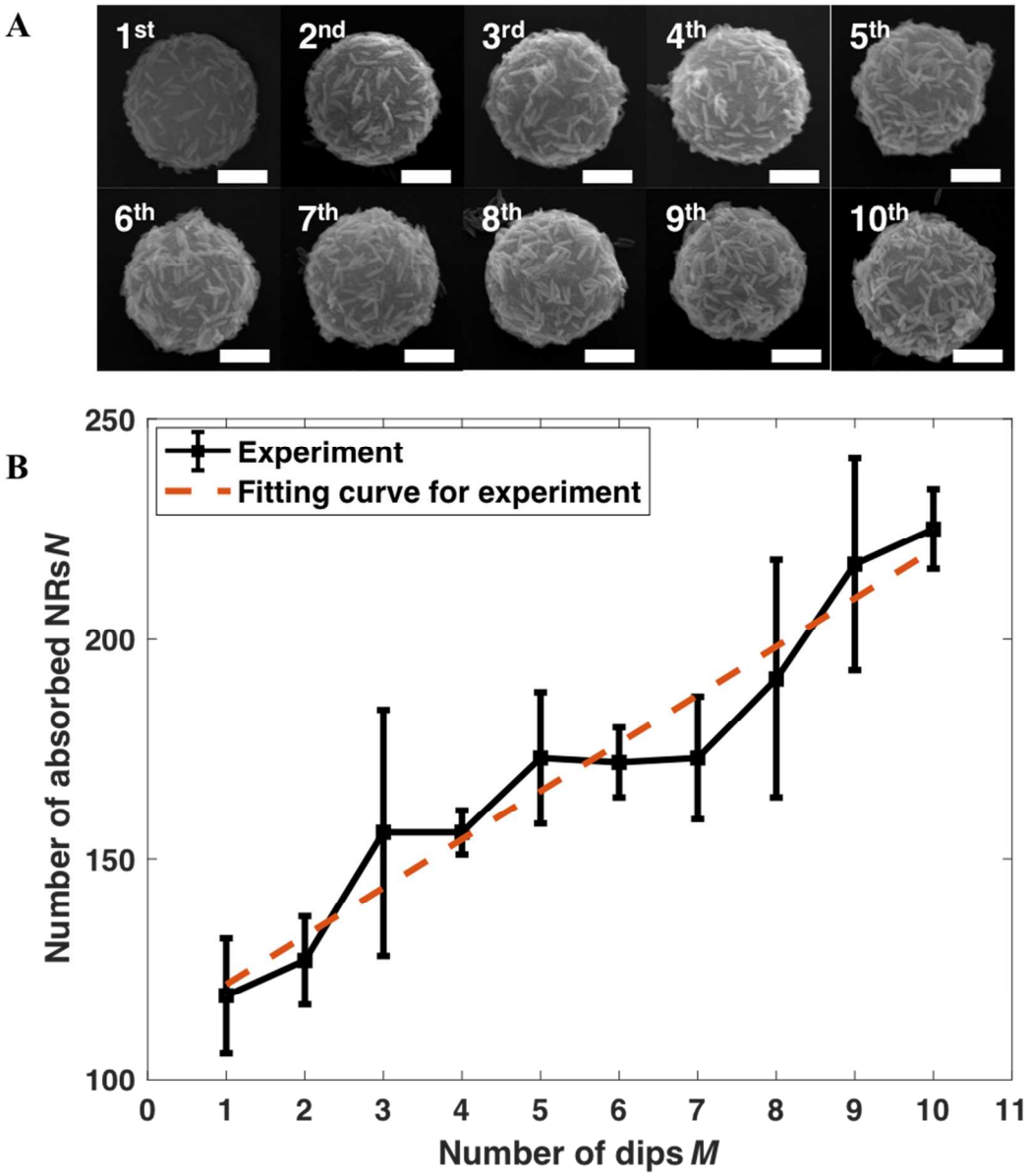

Figure 11. Multilayer NRs deposition: (A) SEM images of the microsphere with different dips. The scale bar for all images is 1 μm. (B) The plot of the number of NRs versus the number of dips *M* based on experimental data. The solid line represents the experimental result and the dash line represents the fitting result.

Conclusions

In summary, we have performed both molecular dynamics simulations and experiments to investigate the LbL assembly of charged NRs onto an oppositely-charged MS in the solvent. We find that due to electrostatic attraction, the charged NRs can spontaneously adsorb to oppositely

charged MS. The concentration, charge density, and shape of the nanoparticle as well as the adsorption time play an important role in the number of adsorbed particles and the final adsorbate coverage on the MS surface. Although in simulation there is a transient time for the number of adsorbed NRs to achieve an equilibrium stage, in experiments, this time is found to be less than 2 min. A classical Langmuir adsorption model can be used to explain the equilibrium adsorbed NRs versus NR concentration, and the results is confirmed by the experiment. For multiple layer deposition, we find that in simulation the formation and morphologies of LbL assembly structures are highly dependent on NR's concentration and the number of dips, but experimentally we failed to create close packed multilayer coating. Our simulation results unveil the microscopic mechanism of the LbL assembly process and provide some useful design guidelines for complex functional superparticles.

Acknowledgements

The authors acknowledge support from the National Science Foundation (Grant. No. CMMI-1306065) and the University of Georgia (UGA) start-up fund. The facility support for modeling and simulations from the UGA Advanced Computing Resource Center are greatly appreciated.

Additional Information

Competing financial interests: The authors declare no competing financial interests.

References

1. Izquierdo, A.; Ono, S. S.; Voegel, J. C.; Schaaf, P.; Decher, G., Dipping versus Spraying: Exploring the Deposition Conditions for Speeding Up Layer-by-Layer Assembly. *Langmuir* **2005,** *21* (16), 7558-7567.
2. Kolasinska, M.; Krastev, R.; Gutberlet, T.; Warszynski, P., Layer-by-Layer Deposition of Polyelectrolytes. Dipping versus Spraying. *Langmuir* **2009,** *25* (2), 1224-1232.
3. Alem, H.; Blondeau, F.; Glinel, K.; Demoustier-Champagne, S.; Jonas, A. M., Layer-by-Layer Assembly of Polyelectrolytes in Nanopores. *Macromolecules* **2007,** *40* (9), 3366-3372.
4. Decher, G., Fuzzy nanoassemblies: Toward layered polymeric multicomposites. *Science* **1997,** *277* (5330), 1232-1237.
5. Carrillo, J.-M. Y.; Dobrynin, A. V., Layer-by-Layer Assembly of Charged Nanoparticles on Porous Substrates: Molecular Dynamics Simulations. *ACS Nano* **2011,** *5* (4), 3010-3019.
6. Andres, C. M.; Kotov, N. A., Inkjet Deposition of Layer-by-Layer Assembled Films. *Journal of the American Chemical Society* **2010,** *132* (41), 14496-14502.
7. Ariga, K.; Hill, J. P.; Ji, Q., Layer-by-layer assembly as a versatile bottom-up nanofabrication technique for exploratory research and realistic application. *Physical Chemistry Chemical Physics* **2007,** *9* (19), 2319-2340.
8. De Villiers, M. M.; Otto, D. P.; Strydom, S. J.; Lvov, Y. M., Introduction to nanocoatings produced by layer-by-layer (LbL) self-assembly. *Adv Drug Deliver Rev* **2011,** *63* (9), 701-715.
9. Pawar, A. B.; Kretzschmar, I., Fabrication, assembly, and application of patchy particles. *Macromolecular rapid communications* **2010,** *31* (2), 150-168.
10. Wang, D.; Rogach, A. L.; Caruso, F., Semiconductor quantum dot-labeled microsphere bioconjugates prepared by stepwise self-assembly. *Nano Lett* **2002,** *2* (8), 857-861.
11. Caruso, F.; Caruso, R. A.; Möhwald, H., Nanoengineering of inorganic and hybrid hollow spheres by colloidal templating. *Science* **1998,** *282* (5391), 1111-1114.
12. Caruso, F., Nanoengineering of particle surfaces. *Advanced materials* **2001,** *13* (1), 11-22.
13. Wang, H.; Sun, L.; Li, Y.; Fei, X.; Sun, M.; Zhang, C.; Li, Y.; Yang, Q., Layer-by-layer assembled Fe3O4@ C@ CdTe core/shell microspheres as separable luminescent probe for sensitive sensing of Cu2+ ions. *Langmuir* **2011,** *27* (18), 11609-11615.
14. Han, Y.; Sukhishvili, S.; Du, H.; Cefaloni, J.; Smolinski, B., Layer-by-layer self-assembly of oppositely charged Ag nanoparticles on silica microspheres for trace analysis of aqueous solutions using surface-enhanced Raman scattering. *Journal of nanoscience and nanotechnology* **2008,** *8* (11), 5791-5800.
15. Derveaux, S.; De Geest, B. G.; Roelant, C.; Braeckmans, K.; Demeester, J.; De Smedt, S. C., Multifunctional layer-by-layer coating of digitally encoded microparticles. *Langmuir* **2007,** *23* (20), 10272-10279.

16. Fakhrullin, R. F.; Lvov, Y. M., "Face-lifting" and "make-up" for microorganisms: layer-by-layer polyelectrolyte nanocoating. *Acs Nano* **2012,** *6* (6), 4557-4564.

17. Park, J. H.; Hong, D.; Lee, J.; Choi, I. S., Cell-in-shell hybrids: chemical nanoencapsulation of Individual cells. *Accounts of chemical research* **2016,** *49* (5), 792-800.

18. Ai, H.; Fang, M.; Jones, S. A.; Lvov, Y. M., Electrostatic layer-by-layer nanoassembly on biological microtemplates: platelets. *Biomacromolecules* **2002,** *3* (3), 560-564.

19. Yang, S. H.; Lee, K. B.; Kong, B.; Kim, J. H.; Kim, H. S.; Choi, I. S., Biomimetic encapsulation of individual cells with silica. *Angewandte Chemie International Edition* **2009,** *48* (48), 9160-9163.

20. Drachuk, I.; Calabrese, R.; Harbaugh, S.; Kelley-Loughnane, N.; Kaplan, D. L.; Stone, M.; Tsukruk, V. V., Silk Macromolecules with Amino Acid–Poly (Ethylene Glycol) Grafts for Controlling Layer-by-Layer Encapsulation and Aggregation of Recombinant Bacterial Cells. *Acs Nano* **2015,** *9* (2), 1219-1235.

21. Acevedo-Fani, A.; Salvia-Trujillo, L.; Soliva-Fortuny, R.; Martín-Belloso, O., Modulating Biopolymer Electrical Charge to Optimize the Assembly of Edible Multilayer Nanofilms by the Layer-by-Layer Technique. *Biomacromolecules* **2015,** *16* (9), 2895-2903.

22. Zelikin, A. N.; Li, Q.; Caruso, F., Degradable polyelectrolyte capsules filled with oligonucleotide sequences. *Angewandte Chemie International Edition* **2006,** *45* (46), 7743-7745.

23. Monika, S., Layered polyelectrolyte complexes: physics of formation and molecular properties. *Journal of Physics: Condensed Matter* **2003,** *15* (49), R1781.

24. Di Michele, L.; Varrato, F.; Kotar, J.; Nathan, S. H.; Foffi, G.; Eiser, E., Multistep kinetic self-assembly of DNA-coated colloids. *Nat Commun* **2013,** *4*.

25. Lawson, R. A.; Peters, A. J.; Ludovice, P. J.; Henderson, C. L. In *Coarse grained molecular dynamics model of block copolymer directed self-assembly*, 2013; pp 86801Y-86801Y-11.

26. Yan, L.-T.; Xie, X.-M., Computational modeling and simulation of nanoparticle self-assembly in polymeric systems: Structures, properties and external field effects. *Progress in Polymer Science* **2013,** *38* (2), 369-405.

27. Perilla, J. R.; Goh, B. C.; Cassidy, C. K.; Liu, B.; Bernardi, R. C.; Rudack, T.; Yu, H.; Wu, Z.; Schulten, K., Molecular dynamics simulations of large macromolecular complexes. *Current Opinion in Structural Biology* **2015,** *31*, 64-74.

28. Petersen, M. K.; Lechman, J. B.; Plimpton, S. J.; Grest, G. S.; in 't Veld, P. J.; Schunk, P. R., Mesoscale hydrodynamics via stochastic rotation dynamics: Comparison with Lennard-Jones fluid. *The Journal of Chemical Physics* **2010,** *132* (17), 174106.

29. Malevanets, A.; Kapral, R., Mesoscopic model for solvent dynamics. *The Journal of Chemical Physics* **1999,** *110* (17), 8605-8613.

30. Lee, Y. S., *Self-Assembly and Nanotechnology Systems: Design, Characterization, and Applications*. Wiley: 2011.

31. Plimpton, S., Fast Parallel Algorithms for Short-Range Molecular Dynamics. *J. Comput. Phys.* **1995,** *117* (1), 1-19.

32. Donath, E.; Walther, D.; Shilov, V.; Knippel, E.; Budde, A.; Lowack, K.; Helm, C.; Möhwald, H., Nonlinear hairy layer theory of electrophoretic fingerprinting applied to consecutive layer by layer polyelectrolyte adsorption onto charged polystyrene latex particles. *Langmuir* **1997,** *13* (20), 5294-5305.

33. Sukhorukov, G. B.; Donath, E.; Lichtenfeld, H.; Knippel, E.; Knippel, M.; Budde, A.; Möhwald, H., Layer-by-layer self assembly of polyelectrolytes on colloidal particles. *Colloids and Surfaces A: physicochemical and engineering aspects* **1998,** *137* (1-3), 253-266.

34. Vincent, B.; Young, C. A.; Tadros, T. F., Adsorption of small, positive particles onto large, negative particles in the presence of polymer. Part 1.-Adsorption isotherms. *Journal of the Chemical Society, Faraday Transactions 1: Physical Chemistry in Condensed Phases* **1980,** *76* (0), 665-673.

1 TOC

2

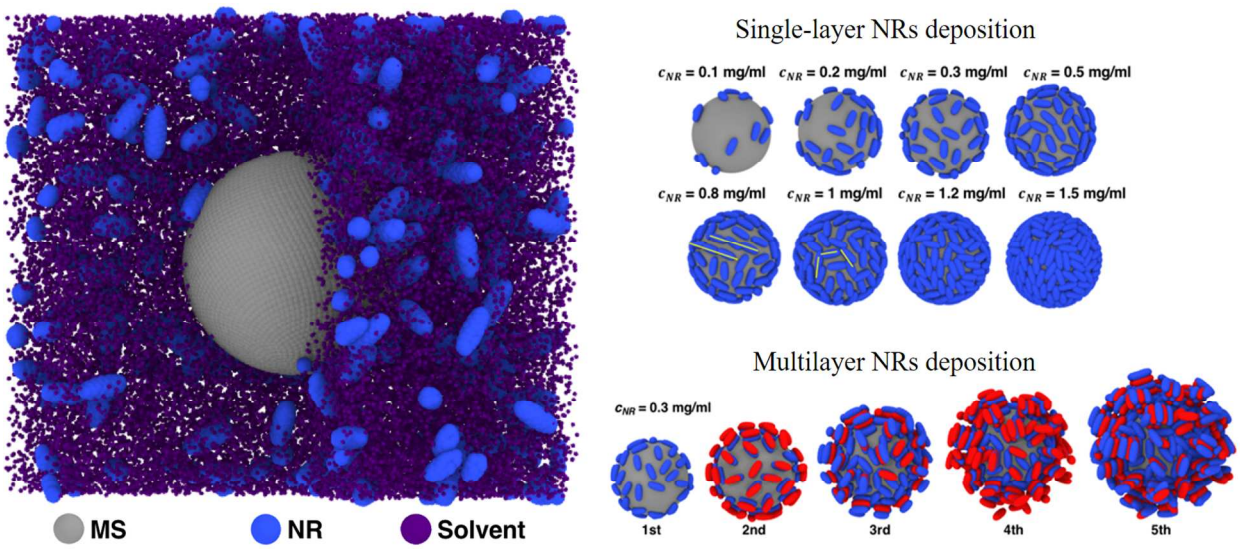
MS
NR
Solvent
Single-layer NRs deposition
c_{NR} = 0.1 mg/ml
c_{NR} = 0.2 mg/ml
c_{NR} = 0.3 mg/ml
c_{NR} = 0.5 mg/ml
c_{NR} = 0.8 mg/ml
c_{NR} = 1 mg/ml
c_{NR} = 1.2 mg/ml
c_{NR} = 1.5 mg/ml
Multilayer NRs deposition
c_{NR} = 0.3 mg/ml
1st
2nd
3rd
4th
5th

3

4